GEVO: Memory-Efficient Monocular Visual Odometry Using Gaussians

Dasong Gao*, Peter Zhi Xuan Li*, Vivienne Sze, Sertac Karaman

Abstract— Constructing a high-fidelity representation of the 3D scene using a monocular camera can enable a wide range of applications on mobile devices, such as micro-robots, smartphones, and AR/VR headsets. On these devices, memory is often limited in capacity and its access often dominates the consumption of compute energy. Although Gaussian Splatting (GS) allows for high-fidelity reconstruction of 3D scenes, current GS-based SLAM is not memory efficient as a large number of past images is stored to retrain Gaussians for reducing catastrophic forgetting. These images often require two-orders-of-magnitude higher memory than the map itself and thus dominate the total memory usage. In this work, we present GEVO, a GS-based monocular SLAM framework that achieves comparable fidelity as prior methods by rendering (instead of storing) them from the existing map. Novel Gaussian initialization and optimization techniques are proposed to remove artifacts from the map and delay the degradation of the rendered images over time. Across a variety of environments, GEVO achieves comparable map fidelity while reducing the memory overhead to around 58 MBs, which is up to $94\times$ lower than prior works.

I. INTRODUCTION

Energy-constrained mobile devices, such as micro-robots, smartphones, AR/VR headsets, enable a wide range of applications from gaming to autonomous exploration. Many applications involve long-term and safe interactions with 3D environments, which require its high fidelity representation constructed using images from cameras. Since mobile devices have limited battery capacity, they often rely on low-power passive sensors to perceive the environment. Thus, we investigate the problem of online simultaneous localization and mapping (SLAM) that can construct a *high fidelity* 3D map using a *monocular* RGB camera on these devices.

On mobile devices, memory is often limited in capacity and its access could dominate the total compute energy. For instance, the energy for accessing data in an 8 KB cache is $10\times$ more than performing a 32-bit floating point multiplication [1]. Furthermore, the energy for accessing data in off-chip DRAM (GBs of capacity) is orders of magnitude higher than that for on-chip cache (KBs to MBs of capacity) [1]. Thus, we are interested in algorithms that are *memory-efficient* with low memory usage so that variables can be effectively cached on the chip to reduce energy.

Constructing a high-fidelity map requires RGB images to guide its optimization process. To achieve real-time operation, many SLAM frameworks [4], [5], [6], [7] optimize the pose and map using a small sliding window of images.

(a) Reconstruction before catastrophic forgetting

(b) MonoGS [2] no past images 8 images stored (7 MB)

(c) GEVO (This work) 8 images stored (7 MB)
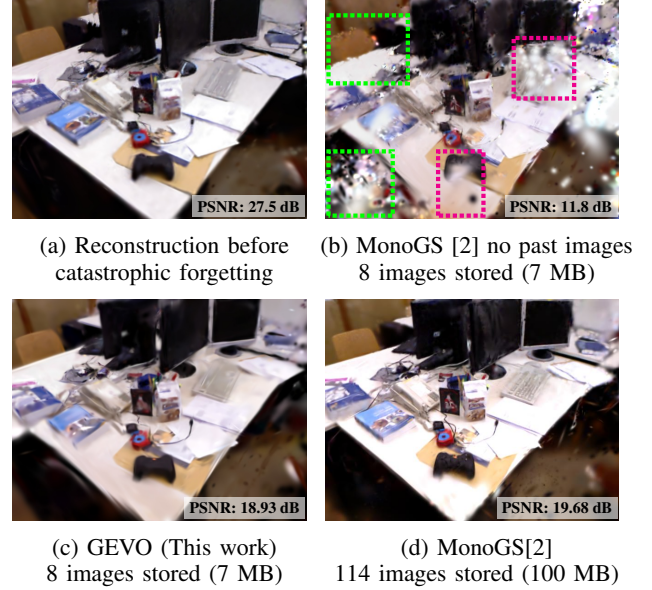
(d) MonoGS[2] 114 images stored (100 MB)

Fig. 1: During online SLAM, the map is optimized using a sliding window buffer of images. a) The region visible during the current sliding window achieves high fidelity after initial optimization. b) However, without storing and retraining the map on a large number of past images, the fidelity of the same region degrades over time due to forgetting (artifacts in rectangles). c) While alleviating forgetting, our GEVO avoids storing past images to reduce the memory overhead. d) To achieve similar map fidelity, MonoGS [3] stores all past keyframes and incurs a memory overhead at least $50\times$ higher than the size of the map.

However, for dense SLAM, the map tends to catastrophically forget and degrade over time after the sliding window has passed (see Figure 1a vs. 1b). To alleviate forgetting, both neural [8], [9], [10] and Gaussian Splatting (GS) [3], [11] based methods *additionally* store a large number of past images outside the current sliding window to repeatedly retrain the map. Unfortunately, the overhead memory used to store these images dominates the total memory and is orders of magnitude higher than both the current sliding window and the map itself.

In particular, catastrophic forgetting in GS-based frameworks occurs when existing Gaussians are: i) *occluded* by new Gaussians constructed in the current sliding window (see red rectangles in Figure 1b), or ii) altered to *overfit* to images in the current sliding window (see green rectangles in Figure 1b). Prior works [2], [9], [12] resolve both factors by retraining all Gaussians using the original camera images

from both the current and past sliding windows.

Our contribution is a memory-efficient SLAM framework, called GEVO, that significantly reduces memory overhead by *rendering* past images from the existing map instead of storing them in memory. However, the fidelity of these rendered images is lower than the original and can slowly degrade overtime due to the artifacts in the map caused by forgetting. Thus, using these images to guide GS optimization alone is insufficient for constructing a high fidelity map. To ensure that rendered images retain high fidelity, we propose novel GS initialization and optimization procedures to further reduce instances of occlusion and overfitting caused by catastrophic forgetting as follows:

1) **Occupancy-Preserving Initialization**: To reduce incorrect occlusions, Gaussians that lie within the obstacle-free regions (*i.e.*, orange Gaussian in the blue region of Figure 2a) are pruned. Thus, in addition to representing obstacles, Gaussians representing free regions are initialized to identify incorrect occlusions.

2) **Consistency-Aware Optimization:** To reduce overfitting of the map to the current window, we only optimize a small subset of Gaussians that are both inconsistent and sufficiently visible to the camera (see orange Gaussians in Figure 2b). To ensure rendered images maintain high fidelity, we locally optimize noisy Gaussians created from the current sliding window before merging them to the map for global optimization.

Across a variety of environments, GEVO achieves comparable map fidelity (see Figure 1c) and reduces the memory overhead to around 58MBs, which is up to $94\times$ lower than prior works. Thus, GEVO makes a significant stride towards the deployment of GS-based SLAM on mobile devices.

II. RELATED WORK

Monocular SLAM frameworks can be classified based on the type of scene representation (*e.g.*, points, planes, neural networks, Gaussians). Constructing these representations online exhibits different trade-offs in computational efficiency, memory overhead, and fidelity.

Traditional Monocular SLAM: Traditional SLAM frameworks can be classified as *indirect* or *direct*, and excel at real-time localization by tracking and optimizing over a set of points representing the 3D scene. For *indirect* frameworks [4], [5], [6], [7], the set of points are selected using feature extractors [13], [14], [15] that seek to uniquely identify certain characteristics of the environment such as corners. Even though these frameworks are often memory-efficient and real-time, the amount of unique features is very sparse which produces a map with very low coverage of the environment and thus cannot be directly used for most downstream applications. In contrast, *direct* frameworks [16], [17], [18], [19] seek to track a denser set of points that have a high photometric gradient in each image at the expense of larger memory and computational overhead. Even though the coverage of the environment increases, reconstruction is still too sparse to appear photorealistic and exhibits a significant amount of noise in regions with less texture [7].

To reduce sparsity, other traditional frameworks explore more descriptive geometric primitives, such as planes [20], quadrics [21] and meshes [22]. However, these frameworks coarsely track the locations of objects that conform to their respective primitives and thus struggle with modeling remaining objects in the scene that do not conform.

Neural Monocular SLAM: To provide a photo-realistic reconstruction of the environment, neural-based SLAM frameworks, such as GO-SLAM [12], NICER-SLAM [10], and iMODE [9] were proposed to represent the environment using a Neural Radiance Field (NeRF). Due to the volumetric rendering required for training NeRFs, Neural SLAM frameworks tend to be computationally intensive. Thus, most of these frameworks focus on developing techniques that accelerate throughput. Some of these techniques include i) using a hybrid scene representation with the voxel grids (in NICER-SLAM) or hash table (in GO-SLAM), and ii) training on a carefully selected subset of input images (in most prior works including iMODE).

Even though throughput was enhanced by these techniques, almost all Neural SLAM frameworks suffer from *catastrophic forgetting*, which is reduced by periodic retraining on images acquired throughout the entire experiment. Thus, these images need to be stored as overhead in memory, which quickly grows with the duration of the experiment to dominate the total memory usage.

Gaussian Monocular SLAM: To improve throughput while maintaining photo-realistic rendering, recent frameworks, such as MonoGS [2], Photo-SLAM [23], and Splat-SLAM [24], deploy Gaussian Splatting (GS) to reconstruct 3D scene from images. While all these frameworks use Gaussians to represent the environment, they deploy different techniques for achieving near real-time localization. For instance, both MonoGS and SplatSLAM localize the camera against the global map via minimizing a photometric cost function, while Photo-SLAM utilizes ORB-SLAM [4].

Similar to Neural SLAM, current Gaussian SLAM frameworks also suffer from *catastrophic forgetting*. In fact, a large number of images from both the current and past sliding window are stored in memory so that they can be used to periodically retrain all Gaussians. In this work, we propose memory-efficient techniques that reduce catastrophic forgetting in GS-based frameworks *without* storing past images. From Figure 1, our framework, named GEVO, can achieve comparable rendering accuracy while requiring significantly less memory overhead compared with prior frameworks.

III. PROPOSED METHODS

In this section, we present GEVO, a memory-efficient GS-based monocular SLAM framework, that reduces *catastrophic forgetting* by relying on images rendered from the map to guide the GS optimization process. Recall that online SLAMs operate on a sliding window of images for localization and mapping. Catastrophic forgetting can occur when Gaussians created from the current window *occlude* the ones from the past windows. As illustrated in Figure 2a, the inconsistency is caused by retrospective occlusion (RO)
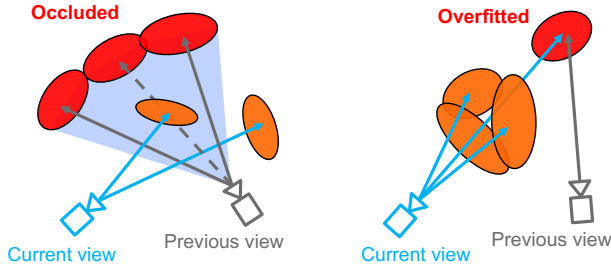
(a) **RO:** The current view inconsistently inserts or moves a new Gaussian into the obstacle-free region of previous views to *occlude* the existing Gaussians.

(b) **IRO**: Sensor rays of the current view pass through new Gaussians to cause *overfitting* of an existing Gaussian created from previous view.

Fig. 2: Two scenarios that cause catastrophic forgetting in Gaussian Splatting: b) retrospective occlusion (RO) and a) incomplete ray obscuration (IRO). RO causes the new Gaussians to occlude ones in the past view (red rectangles in Figure 1b). IRO causes the existing Gaussians to overfit to the current view (green rectangles in Figure 1b).

where Gaussians from the current view (orange) lie within the obstacle-free region (blue) of the prior view.

Catastrophic forgetting can also occur when a previously observed region from a past sliding window *overfit* to images from the current sliding window. As illustrated in Figure 2b, overfitting is caused by incomplete ray obscuration (IRO) where Gaussians that are associated with the current view (red) do not completely obscure the sensor rays (blue). Thus, Gaussians created from prior views (orange) are still partially visible such that their parameters update to match the appearances in the current view. In prior works, both RO and IRO are reduced by storing images from all sliding windows to retrain the Gaussians. These images typically dominate the total memory usage which grows over time.

Replacing images from the past sliding window with the ones *rendered* from the existing map is not sufficient for reducing catastrophic forgetting. In particular, the fidelity of these images slowly degrades over time due to artifacts in the map caused by forgetting. Thus, our framework deploys techniques that reduce forgetting throughout the entire Gaussian initialization and optimization process. To reduce RO, our framework consists of an accurate Gaussian initialization procedure (Section III-A) that compactly encodes obstacle-free regions. These regions are used to identify instances where new Gaussians occlude existing ones, which are pruned at the end of optimization. To reduce IRO, we propose a two-stage optimization procedure (Section III-B) to update a small subset of Gaussians that are both inconsistent and sufficiently visible to the current sliding window so that the remaining Gaussians do not overfit to the current window.

A. Occupancy-Preserving Initialization

In this section, we present an efficient procedure that initializes Gaussian parameters representing obstacles and obstacle-free regions in the current sliding window. The

obstacle-free regions are used to prune Gaussians that causes RO (Figure 2a).

To achieve computational efficiency and good generalization across a variety of environments, our procedure is adapted from an efficient implementation of multi-view stereo [26] and does not rely on time-consuming COLMAP [27], [28] or less accurate random sampling [2]. Figure 3 summarizes our procedure. Given a sequence of RGB keyframes in a sliding window, we construct a cost volume that captures the photometric consistency for each pixel in the most recent image at different depth hypotheses. From the cost volume, belief propagation [29] is performed to extract a depth image associated with the most recent image. Finally, Gaussian parameters for both obstacles (red) and free regions (blue) are efficiently computed by the memory-efficient SPGF* algorithm [25].

Our procedure can be integrated with many localization and keyframe selection strategies, such as map-centric direct methods in MonoGS [2] and feature-based methods in ORB-SLAM [4]. Details about our procedure are described below.

1) Cost Volume Generation: Given a sequence of $N = 8$ or 10 keyframes $(I_0, \ldots, I_{N-1})$ from the sliding window buffer (with I_{N-1} being the most recent), the value of the photometric cost $V(\mathbf{u}, d)$ for pixel $\mathbf{u}$ in I_{N-1} when depth is hypothesized to be d is defined as

$$V(\mathbf{u}, d) = \frac{1}{N-1} \sum_{i=0}^{N-2} |I_{N-1}(\mathbf{u}) - I_i\left(\pi(\mathbf{u}, d, \mathbf{T}_{N-1}^i)\right)|, \tag{1}$$

where $I(\cdot)$ is the intensity of a specific pixel in image I, $\mathbf{T}_{N-1}^i \in \mathbb{SE}(3)$ is the transformation matrix from image I_{N-1} to I_i, $\pi(\cdot)$ wraps the coordinate $\mathbf{u}$ from image I_{N-1} to I_i given the depth hypotheses d.

In our experiments, we choose 64 depth hypothesis (*i.e.*, $\{d_0, \ldots, d_{63}\}$ in Figure 3) that are equally spaced from $0.25 - 25$ m. To reduce memory overhead, we downsample the image by $4\times$ in each dimension before creating the cost volume in order to exploit the spatial redundancy in the image. Assuming that each image has height $H = 480$ and width $W = 640$, the resulting cost volume V only requires 4.7MBs. The potential loss in spatial details will be recovered via upsampling in Section III-A.2.

2) Gaussian Generation: Recall that the cost volume generated in Equation (1) contains 64 depth hypotheses with different photometric costs for each pixel. To determine the most likely depth for each pixel under the assumption that each obstacle has smooth surfaces, we used belief propagation (BP) from [29] to extract a depth image for the most recent keyframe in the sliding window buffer. Under the assumption that neighboring pixels with the same color in the keyframe are likely to describe the same surface, we use an efficient algorithm proposed in [30] to upsample the depth image from BP to the full resolution of the keyframe.

Given the most recent keyframe and its depth image, we enhanced a memory-efficient algorithm, called SPGF* [25], to generate a set of Gaussians representing obstacles (red) and free (blue) regions (see Figure 3). Unlike prior ap-
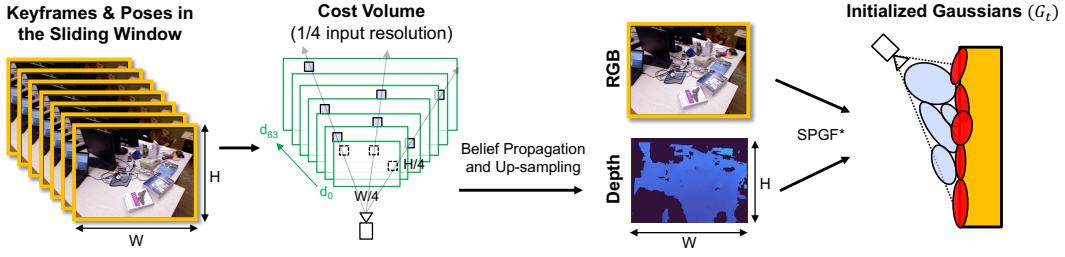
Fig. 3: **Occupancy-Preserving Initialization.** Given a set of recently acquired keyframes and poses in a sliding window buffer, the depth image for the most recent keyframe is computed using belief propagation on a photometric cost volume at a quarter of the image's resolution. Then, the depth and RGB image are used to initialize a set of Gaussians ($\mathcal{G}_t$) for representing obstacles (red) and free region (blue) using the SPGF* algorithm [25]. Gaussians representing free regions are fused across multiple keyframes to identify instances of retrospective occlusion (RO) during consistency-aware optimization.
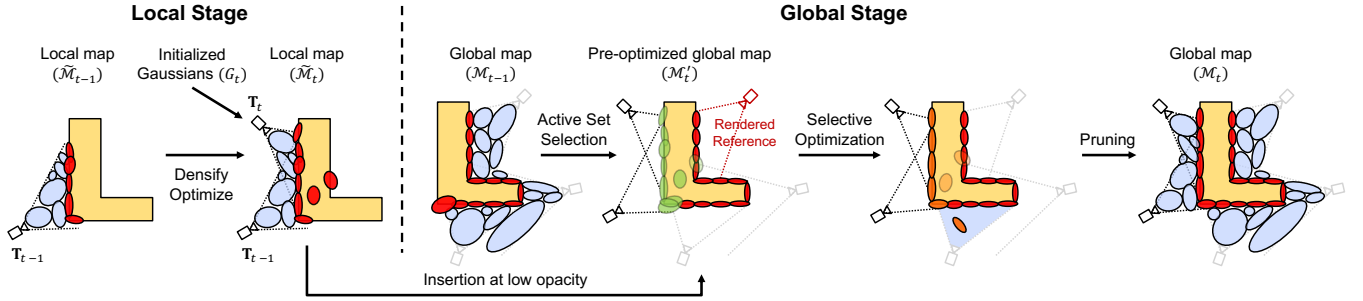

Fig. 4: **Consistency-Aware Optimization.** Given newly initialized Gaussians ($\mathcal{G}_t$), we perform a GS-based optimization in two stages: i) *Local stage* performs GS to optimize a local map $\widetilde{\mathcal{M}}_t$ that represents all geometries visible from the sliding window, and ii) *Global stage* selectively optimizes a small active set $\mathcal{A}_t$ of Gaussians (green) consisting of the local map $\widetilde{\mathcal{M}}_t$ and existing Gaussians $\mathcal{E}_t$ with high rendering error. This active set selection tends to exclude Gaussians obscured from camera views used for training and thus reduces IRO. Since Gaussians from the local map are sufficiently accurate, images from randomly selected past views are *rendered* from the global map to guide the global optimization stage. Finally, Gaussians that causes RO are pruned with the help of the obstacle-free regions created during initialization (blue). Note that Gaussians representing free regions are omitted in the global stage except for the pruning step for ease of visualization.

proaches [31], [32], [33], [34] that process the depth image in multiple passes, SPGF* exploits the connectivity encoded in the depth image to efficiently generate the Gaussians in a single pass with comparable accuracy. Since SPGF* was mainly designed for accurate depth reconstruction, each Gaussian that represents an obstacle could enclose a surface containing multiple colors. To enhance the fidelity of color representation, we modified SPGF* to ensure that each Gaussian can only represent a surface with a similar color.

B. Consistency-Aware Optimization

After Gaussians are initialized in Section III-A, they are fused into the global map as illustrated in Figure 4. Recall that our initialization procedure constructs a set of Gaussians ($\mathcal{G}_t$) representing both the obstacles and free regions that are visible from the current keyframe. Two challenges arise when integrating the new Gaussians into the existing map using the current sliding window: i) Since these Gaussians are potentially noisy, their insertion into the map likely causes RO; ii) During optimization, both IRO and RO tend to occur due to the lack of constraint from past views. In prior works [23], [12], [2], both are resolved by training Gaussians

on keyframes sampled from past sliding windows. In our work, we rely on past keyframes *rendered* from the existing map to reduce memory overhead.

However, the fidelity of these rendered images degrades over time which leads to significant degradation of the map itself. To maintain the fidelity of these images, we employ a two-stage optimization that first enhances the fidelity of the initialized Gaussians in the local stage before optimizing them with other existing Gaussians in the global stage. Since existing Gaussians are not perturbed during the local stage, we can recover the color of past keyframes with high fidelity through *rendering*. To reduce IRO, we optimize a small subset of Gaussians that are both inconsistent and visible from the current sliding window. In addition, the free space information encoded by past keyframes can be retrieved by querying the Gaussians representing the free region, allowing us to further reduce RO by occupancy-based pruning.

1) Local Stage: During the local stage, the initialized Gaussians $\mathcal{G}_t$ are appended with other Gaussians $\widetilde{\mathcal{M}}_{t-1}$ that are also visible from the current sliding window to form an updated local map $\widetilde{\mathcal{M}}_t$. Since the local map contains recently initialized Gaussians, it is potentially noisy. To enhance its

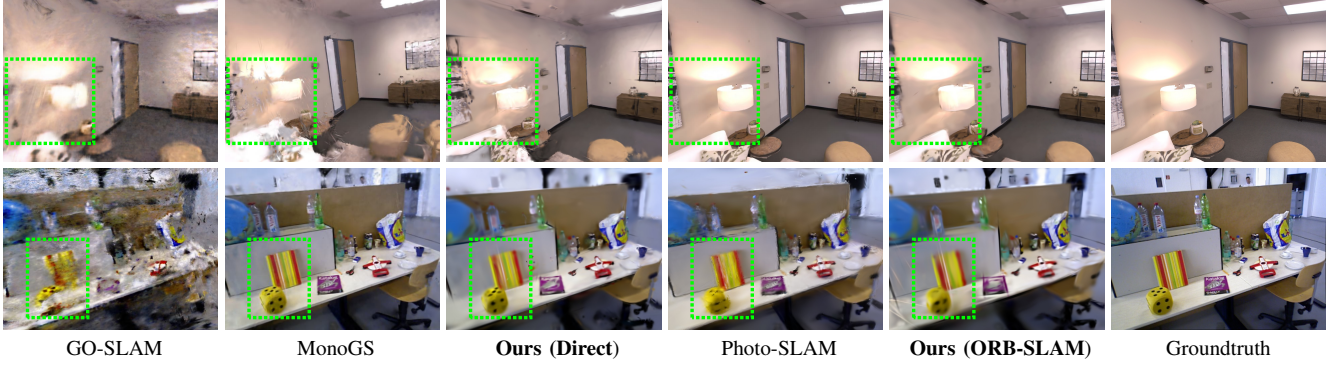| GO-SLAM | MonoGS | **Ours (Direct)** | Photo-SLAM | **Ours (ORB-SLAM)** | Groundtruth |

Fig. 5: Examples of rendering results for GEVO and other monocular methods on Replica and TUM-RGBD. GEVO maintains compatible map fidelity compared with prior works (see regions with high levels of details in green rectangles).

fidelity, it is optimized using images from only the current sliding window via the following cost function [2],

$$\underset{\mathbf{T}_k, \widetilde{\mathcal{M}}_t}{\arg\min} E_{pho} + E_{iso}, \tag{2}$$

where E_{pho} is the photometric loss between rendered and ground truth images, E_{iso} is the isotropic loss, which prevents the formation of elongated or thin Gaussians, and $\mathbf{T}_k \in \mathbb{SE}(3)$ is its estimated pose.

2) Global Stage: After the Gaussians in local map $\widetilde{\mathcal{M}}_t$ are optimized, they can more accurately represent the environment. To resolve remaining consistencies with prior measurements and enhance the compactness of the map, we merge Gaussians $\widetilde{\mathcal{M}}_t$ into the global map $\mathcal{M}_{t-1}$. During the merging process, we reduce catastrophic forgetting by identifying and updating a small subset of the Gaussians that are temporally inconsistent across past viewpoints by using keyframes *rendered* from these viewpoints. Since the global map $\mathcal{M}_{t-1}$ is not perturbed during the local stage, these rendered keyframes from $\mathcal{M}_{t-1}$ maintain high quality and are sufficient for resolving the remaining inconsistencies.

The global stage consists of the following three sequential steps: insertion, selective optimization, and pruning. We describe them in detail as follows.

Insertion and activation: We insert the local map $\widetilde{\mathcal{M}}_t$ and the previous global map $\mathcal{M}_{t-1}$ to create the pre-optimzied global map: $\mathcal{M}'_t \leftarrow \widetilde{\mathcal{M}}_t \cup \mathcal{M}_{t-1}$. To prevent retrospective occlusion (RO) caused by local map $\widetilde{\mathcal{M}}_t$, we lower its opacity to 0.2 prior to the insertion.

Selective optimization: We employ an optimization procedure similar to Equation (2) but with two modifications: 1) To prevent Gaussians in the pre-optimized map $\mathcal{M}'_t$ from overfitting to the images from the current sliding window buffer $\mathcal{W}_t$, we select and only optimize an active subset $\mathcal{A}_t \subseteq \mathcal{M}'_t$, and 2) we additionally introduce a photometric consistency loss E_{pc} to further ensure consistency with the prior global map $\mathcal{M}_{t-1}$. The overall objective is therefore:

$$\underset{\mathbf{T}_k, \mathcal{A}_t}{\arg\min} E_{pho} + E_{iso} + E_{pc}. \tag{3}$$

Specifically, we choose $\mathcal{A}_t = \widetilde{\mathcal{M}}_t \cup \mathcal{E}_t$, which contains the newly inserted Gaussians and a subset $\mathcal{E}_t$ that incurs high rendering error in the current window:

$$\mathcal{E}_t = \left\{ g \in \mathcal{M}_{t-1} : \max_{k \in \mathcal{W}_t} E_k(g) > \epsilon \right\}, \tag{4}$$

where the per-Gaussian rendering error $E_k(g)$ as in [35]:

$$E_k(g) = \sum_{\mathbf{u}} w(g, \mathbf{u}) |R(\mathcal{M}_{t-1}, \mathbf{T}_k)(\mathbf{u}) - C_k(\mathbf{u})|, \tag{5}$$

with $\mathbf{u}$ being the pixel coordinate, and $w(g, \mathbf{u})$ is the alpha-blending coefficient of g at pixel $\mathbf{u}$. Since the Gaussians that are more visible to the camera contribute more to $E_k(g)$, the active set tends to exclude existing Gaussians that are not well-observed by the current window and reduce IRO.

To further ensure that the fidelity of the global map does not degrade over time, the objective in Equation (3) includes a photometric consistency loss E_{pc} evaluated on keyframes at four past camera views outside the sliding window:

$$E_{pc} = \sum_{l=1}^{4} \left\| R(\mathcal{M}'_t, \mathbf{T}_{k_l}) - \cancel{\nabla}(R(\mathcal{M}_{t-1}, \mathbf{T}_{k_l})) \right\|_1, \tag{6}$$

where $R(\cdot)$ is the rendering function, frame index k_l is uniformly sampled from past timesteps $1 \ldots t - W$, and $\cancel{\nabla}(\cdot)$ is the stop gradient operator [35], which avoids back-propagating gradient through $R(\mathcal{M}_{t-1}, \mathbf{T}_{k_l})$.

Pruning: After selective optimization, we prune updated Gaussians still causing RO. These Gaussians are identified by having a) an opacity less than 0.7 or b) an occupancy probability less than 0.9. The occupancy probability is computed using Gaussian Mixture Regression [25] on the initialized Gaussians representing free regions from Section III-A.

IV. EXPERIMENTS

In this section, we evaluate our GEVO framework against state-of-the-art (SOTA) monocular dense SLAMs in terms of accuracy and memory overhead. To further demonstrate the trade-offs among different system configurations, we choose the following frameworks: GO-SLAM[1] [12] (learning-based

---

[1][Online]. Available: https://github.com/youmi-zym/GO-SLAM

TABLE I: Memory usage and rendering accuracy of GEVO compared with prior works on scenes from the Replica [36] and TUM RGB-D [37] datasets. The best results are highlighted as first and second .

Metrics	Methods	office0	office1	office2	office3	office4	room0	room1	room2	Average	fr1_desk	fr2_xyz	fr3_office	Average
Overhead Memory (MB) ↓	GO-SLAM	2673.6	2794.6	3066.2	3001.3	2575.7	3606.0	3651.6	3796.0	3145.6	3747.0	2870.8	4087.5	3568.5
	MonoGS	534.6	618.6	664.8	678.4	383.2	697.0	168.2	683.7	553.6	106.7	96.3	213.3	138.8
	Ours (Direct)	**72.8**	**71.1**	**70.5**	**75.5**	**67.6**	**82.3**	**71.2**	**71.6**	**72.8**	**25.1**	**24.2**	**24.3**	**24.6**
	Photo-SLAM	606.2	1504.7	631.1	559.2	633.3	675.1	791.6	650.5	756.5	135.6	336.9	629.3	367.3
	Ours (ORB-SLAM)	85.6	86.1	100.8	93.4	100.3	92.3	95.6	98.5	94.1	40.4	30.7	43.4	38.1
Map Memory (MB) ↓	GO-SLAM	48.1	48.1	48.1	48.1	48.1	48.1	48.1	48.1	48.1	48.1	48.1	48.1	48.1
	MonoGS	**2.8**	3.1	**4.3**	6.2	**2.4**	9.1	**2.9**	4.4	**4.4**	1.3	2.4	2.1	1.9
	Ours (Direct)	4.6	3.4	6.6	5.9	4.5	9.1	5.8	5.7	5.7	**0.8**	**0.4**	**1.0**	**0.7**
	Photo-SLAM	4.8	10.2	6.4	**4.5**	5.0	9.4	9.0	5.4	6.8	2.1	3.8	5.1	3.6
	Ours (ORB-SLAM)	2.9	**2.1**	5.9	4.9	4.6	**7.3**	5.3	**4.4**	4.7	1.0	0.4	**0.7**	**0.7**
PSNR (dB) ↑	GO-SLAM	28.4	28.2	19.6	22.4	23.9	20.8	24.8	13.2	22.7	16.0	15.7	15.4	15.7
	MonoGS	25.3	29.1	22.0	24.3	15.2	21.9	8.2	22.4	21.1	17.8	14.1	**18.1**	16.7
	Ours (Direct)	24.6	28.7	26.5	25.5	15.9	24.3	20.9	23.9	23.8	17.6	19.8	15.9	17.8
	Photo-SLAM	**35.8**	**37.3**	**30.2**	**30.9**	**33.2**	**29.0**	**31.0**	**32.3**	**32.4**	**20.5**	**23.0**	18.0	**20.5**
	Ours (ORB-SLAM)	33.4	34.6	27.7	28.1	27.5	27.0	28.4	28.3	29.4	18.5	19.8	17.1	18.5
SSIM ↑	GO-SLAM	0.76	0.76	0.63	0.68	0.76	0.54	0.72	0.44	0.66	0.46	0.45	0.44	0.45
	MonoGS	0.67	0.86	0.81	0.82	0.40	0.71	0.16	0.80	0.65	0.66	0.54	**0.67**	0.62
	Ours (Direct)	0.81	0.84	0.85	0.85	0.81	0.78	0.75	0.85	0.82	0.63	0.68	0.61	0.64
	Photo-SLAM	**0.95**	**0.95**	**0.92**	**0.91**	**0.93**	**0.85**	**0.90**	**0.93**	**0.92**	**0.73**	**0.78**	**0.65**	**0.72**
	Ours (ORB-SLAM)	0.91	0.90	0.88	0.88	0.91	0.82	0.86	0.89	0.88	0.65	0.68	0.64	0.66
LPIPS ↓	GO-SLAM	0.46	0.42	0.48	0.49	0.49	0.58	0.50	0.69	0.51	0.56	0.54	0.63	0.57
	MonoGS	0.40	0.28	0.36	0.27	0.59	0.37	0.78	0.38	0.43	0.39	0.49	0.42	0.43
	Ours (Direct)	0.35	0.27	0.27	0.23	0.41	0.26	0.39	0.27	0.31	0.45	0.43	0.56	0.48
	Photo-SLAM	**0.07**	**0.06**	**0.10**	**0.10**	**0.08**	**0.12**	**0.08**	**0.08**	**0.09**	**0.25**	**0.14**	**0.29**	**0.22**
	Ours (ORB-SLAM)	0.20	0.21	0.24	0.20	0.21	0.22	0.22	0.20	0.21	0.43	0.44	0.50	0.46
ATE (cm) ↓	GO-SLAM	**0.3**	0.7	**0.4**	0.5	0.8	0.5	**0.3**	0.3	**0.5**	2.3	**0.3**	1.8	1.5
	MonoGS	40.7	30.5	56.3	19.2	58.3	19.9	32.9	34.7	36.6	2.9	20.8	10.4	11.4
	Ours (Direct)	14.0	12.9	7.8	4.2	187.4	12.3	41.2	7.3	35.9	8.0	2.6	39.1	16.6
	Photo-SLAM	0.6	0.4	1.0	**0.5**	**0.7**	0.4	0.7	**0.2**	0.6	**1.6**	0.4	**1.6**	**1.2**
	Ours (ORB-SLAM)	0.5	**0.3**	1.6	1.0	0.9	0.4	1.6	1.0	0.9	2.9	0.8	2.9	2.2

tracking + neural-based mapping), MonoGS[2] [2] (direct tracking + Gaussian-based mapping), and Photo-SLAM[3] [23] (feature-based tracking + Gaussian-based mapping). Compared with prior methods across multiple environments, GEVO reduces the overhead memory by **8-145×** while maintaining comparable accuracy (See Figure 5).

This section is organized as follows. After presenting the implementation details for all methods and dataset selection in Section IV-A, we compare the memory usage (Section IV-B), rendering and localization accuracy (Section IV-C) against SOTA methods. Finally, an ablation study for the design decisions of GEVO is presented in Section IV-D.

A. Experiment Setup

GEVO is implemented in C++ with CUDA acceleration and can be found at https://github.com/mit-lean/gevo. We benchmarked GEVO and prior methods with an Intel Xeon Gold 6130 and NVIDIA TITAN RTX GPU. We use a sliding window buffer that stores either 8 (TUM) or 10 (Replica) keyframes. For prior methods, we use the default settings from the open-source code release for supported datasets or otherwise perform fine-tuning from default settings.

Our method is compatible with various tracking methods. For fairness, we present results of two variants of GEVO: *Ours (Direct)* employs the photometric tracking from MonoGS whereas *Ours (ORB-SLAM)* uses ORB-SLAM [4] for tracking as in Photo-SLAM. For Photo-SLAM and Ours (ORB-SLAM), we disabled loop closure and downsampled the ORB vocabulary to 1/100 of the original to reduce memory usage without sacrificing accuracy. We disabled spherical harmonics for all GS-based methods.

We benchmarked all frameworks on Replica [37], a highly detailed synthetic dataset that provides noiseless RGB images for estimating the upper bound performance of the methods, and TUM RGB-D [36], a real-world dataset for testing the methods under noisy images from a Kinect camera. Similar to prior works, we select eight sequences from Replica: office_0-4 and room_0-2 and three from TUM RGB-D: fr1_desk, fr2_xyz and fr3_office.

B. Memory Usage

In this section, we present results and analysis on the memory usage of GEVO and the compared frameworks. The total memory is comprised of: 1) the *map*, which is the size of the resulting NeRF or Gaussians, and 2) the *overhead*, which is the extra memory for storing input and temporal variables during the execution in order to produce the output (the map).

Note that the overhead memory is highly dependent on the algorithm and its implementation. To reduce the impact of implementation, we only track variables that are *essential* to the algorithm[4] and avoid ones cached solely for acceleration.

The overhead memory of GEVO and other methods is summarized in Table I. Overall, GEVO requires the lowest average overhead memory of 83.5 MB on Replica and 31.4 MB on TUM, which are dominated by the keyframes stored in the current window. In MonoGS and Photo-SLAM, many keyframes from both current and past windows are stored in memory to periodically train Gaussians to reduce catastrophic forgetting. For these frameworks, the keyframes dominate (96% to 99%) the overhead memory. By only storing images in the current sliding window, GEVO reduces the overhead memory by 114 MB on average on TUM compared with MonoGS and Photo-SLAM. Since the image resolution is $2.65\times$ higher on Replica, GEVO achieves an even higher overhead memory reduction (480 MB on average).

Among the benchmarked methods, GO-SLAM has the highest overhead memory due to the storage of large temporary variables in addition to all keyframe images. Specifically, with a tracker derived from DROID-SLAM, GO-SLAM computes a 4D correlation volume [38] between each pair of pixels of multiple feature maps to obtain the optical flow. With a size of at least 1 GB, the 4D correlation volume contributes to 50% to 60% of the overhead memory. Thus, GEVO reduces the overhead memory by up to $53\times$ on Replica and $168\times$ on TUM compared with GO-SLAM.

From Table I, the map memory of all prior frameworks only consumes a tiny fraction (0.5% to 2.4%) of the total memory. Thus, the total memory in each framework is dominated by the overhead memory, which our framework addresses. Recall that maps in GS-based frameworks (GEVO, MonoGS, and Photo-SLAM) consist of Gaussians whose number scales with the size of the environment. In contrast, GO-SLAM is a neural-based method whose network size cannot adapt to the size of the environment. Thus, the map size of GO-SLAM for both datasets is constant at 48 MB, which is consistently $4.7\times$ to $124\times$ higher than GS-based frameworks for both datasets.

C. Rendering and Localization Accuracy

In this section, we compare the accuracy of GEVO against prior methods. Similar to prior methods, we computed the PSNR, SSIM, and LPIPS metrics between each rendered and original RGB image of every five non-keyframes in addition to reporting the RMSE of average translation error (ATE) of keyframes. As shown in Table I, our framework with ORB-SLAM localization achieves the second-best rendering accuracy and comparable localization accuracy on almost all sequences compared with Photo-SLAM, the best-performing method. By using rendered images from the map in addition to our initialization and optimization procedures, our PSNR degrades by 3 dB on Replica and 2 dB on TUM compared with Photo-SLAM.

---

[4]Measured using our own memory profiler that tracks memory allocation of these variables in their C++ constructors and deconstructors.

TABLE II: Impacts of various techniques in GEVO on the PSNR for the TUM RGB-D dataset. To avoid the impacts of localization error, ground truth poses are used.

Stored References								✓
Rendered References			✓		✓	✓	✓	
Two-Stage Optimization				✓	✓	✓	✓	
Selective Optimization						✓	✓	
Free Space Pruning							✓	
PSNR (dB)	Initial	25.9	25.1	23.8	23.7	22.7	22.6	25.0
	Final	15.5	17.0	16.5	18.4	18.8	19.0	19.4

Since our framework is compatible with many localization methods, we configure our framework using the same direct localization method as MonoGS for its comparison. Due to a more geometrically verified Gaussian initialization procedure based on traditional multi-view stereo, our framework is less likely to incur a large ATE compared with MonoGS, which randomly initializes Gaussians using priors from the global map. Due to our consistency-aware optimization, our framework often yields a better rendering accuracy in more than half of the sequences compared with MonoGS without training on up to 300 keyframes stored in memory.

Figure 5 shows sample rendering from the benchmarked sequences. The rendering of GEVO shows minimal visual difference compared with Photo-SLAM and suffers from fewer artifacts than MonoGS. Despite robust localization, GO-SLAM shows the most noticeable artifacts, especially on TUM, which contains motion blur and lighting changes.

D. Ablation Studies

In this section, we show the impact of our proposed techniques on alleviating catastrophic forgetting. To measure forgetting, we evaluate the rendering PSNR of each keyframe upon its evacuation from the sliding window and after the full sequence is processed, which we label as the initial and final PSNR, respectively. Table II shows the initial and final PSNR averaged across all keyframes of three sequences in the TUM dataset. To avoid the impact of localization on map fidelity, we used the ground truth trajectory.

Without retraining with any images outside the current sliding window (leftmost column of Table II), the rendering quality of keyframes degrades significantly over time due to catastrophic forgetting (see Figure 1b). Simply replacing stored images with rendered ones (column 2) alone noticeably increases the final PSNR. However, since rendered images degrade in fidelity over time, using them alone is not sufficient without additional techniques (columns 3-6). All techniques combined recover the final average PSNR to 19 dB (see Figure 1c), which is only 0.4 dB lower than storing and training with original images (rightmost column). Although each additional technique gradually lowers the initial PSNR due to stronger regularization, they tend to impede forgetting during optimization. Thus, all our techniques combined recover most of the loss in fidelity due to not storing and retraining using the original past images.

V. Conclusion

In this letter, we presented GEVO, a memory-efficient GS-based monocular SLAM that avoids catastrophic forgetting due to incomplete sensor obscuration (IRO) and retrospective occlusion (RO) without storing past images. By using rendered images to guide the optimization and introducing occupancy-preserving initialization and consistency-aware optimization to retain their fidelity, map consistency is maintained throughout the sequence. Experiments on the TUM and Replica datasets show that while maintaining comparable rendering accuracy with SOTA methods, GEVO reduces the memory overhead to 58 MBs, which is up to $94\times$ lower than prior methods. Thus, GEVO has made a significant step towards deploying GS-based SLAM on mobile devices.

References

[1] M. Horowitz, "1.1 computing's energy problem (and what we can do about it)," in *2014 IEEE International Solid-State Circuits Conference Digest of Technical Papers (ISSCC)*, 2014, pp. 10–14.

[2] H. Matsuki, R. Murai, P. H. Kelly, and A. J. Davison, "Gaussian splatting slam," in *Proceedings of the IEEE/CVF Conference on Computer Vision and Pattern Recognition*, 2024, pp. 18 039–18 048.

[3] H. Matsuki, R. Murai, P. H. J. Kelly, and A. J. Davison, "Gaussian Splatting SLAM," in *Proceedings of the IEEE/CVF Conference on Computer Vision and Pattern Recognition*, 2024.

[4] C. Campos, R. Elvira, J. J. G. Rodríguez, J. M. Montiel, and J. D. Tardós, "Orb-slam3: An accurate open-source library for visual, visual–inertial, and multimap slam," *IEEE Transactions on Robotics*, vol. 37, no. 6, pp. 1874–1890, 2021.

[5] C. Forster, L. Carlone, F. Dellaert, and D. Scaramuzza, "On-manifold preintegration for real-time visual–inertial odometry," *IEEE Transactions on Robotics*, vol. 33, no. 1, pp. 1–21, 2016.

[6] A. J. Davison, I. D. Reid, N. D. Molton, and O. Stasse, "Monoslam: Real-time single camera slam," *IEEE transactions on pattern analysis and machine intelligence*, vol. 29, no. 6, pp. 1052–1067, 2007.

[7] R. Mur-Artal and J. Tardos, "Probabilistic semi-dense mapping from highly accurate feature-based monocular slam," in *Proceedings of Robotics: Science and Systems*, Rome, Italy, July 2015.

[8] A. Rosinol, J. J. Leonard, and L. Carlone, "Nerf-slam: Real-time dense monocular slam with neural radiance fields," in *2023 IEEE/RSJ International Conference on Intelligent Robots and Systems (IROS)*. IEEE, 2023, pp. 3437–3444.

[9] H. Matsuki, E. Sucar, T. Laidow, K. Wada, R. Scona, and A. J. Davison, "imode: Real-time incremental monocular dense mapping using neural field," in *2023 IEEE International Conference on Robotics and Automation (ICRA)*. IEEE, 2023, pp. 4171–4177.

[10] Z. Zhu, S. Peng, V. Larsson, Z. Cui, M. R. Oswald, A. Geiger, and M. Pollefeys, "Nicer-slam: Neural implicit scene encoding for rgb slam," in *2024 International Conference on 3D Vision (3DV)*. IEEE, 2024, pp. 42–52.

[11] H. Huang, L. Li, C. Hui, and S.-K. Yeung, "Photo-slam: Real-time simultaneous localization and photorealistic mapping for monocular, stereo, and rgb-d cameras," in *Proceedings of the IEEE/CVF Conference on Computer Vision and Pattern Recognition*, 2024.

[12] Y. Zhang, F. Tosi, S. Mattoccia, and M. Poggi, "Go-slam: Global optimization for consistent 3d instant reconstruction," in *Proceedings of the IEEE/CVF International Conference on Computer Vision*, 2023, pp. 3727–3737.

[13] G. Lowe, "Sift-the scale invariant feature transform," *Int. J*, vol. 2, no. 91-110, p. 2, 2004.

[14] H. Bay, A. Ess, T. Tuytelaars, and L. Van Gool, "Speeded-up robust features (surf)," *Computer vision and image understanding*, vol. 110, no. 3, pp. 346–359, 2008.

[15] E. Rublee, V. Rabaud, K. Konolige, and G. Bradski, "Orb: An efficient alternative to sift or surf," in *2011 International conference on computer vision*. Ieee, 2011, pp. 2564–2571.

[16] J. Engel, T. Schöps, and D. Cremers, "Lsd-slam: Large-scale direct monocular slam," in *European conference on computer vision*. Springer, 2014, pp. 834–849.

[17] R. A. Newcombe, S. J. Lovegrove, and A. J. Davison, "Dtam: Dense tracking and mapping in real-time," in *2011 International Conference on Computer Vision*, 2011, pp. 2320–2327.

[18] G. Klein and D. Murray, "Parallel tracking and mapping for small ar workspaces," in *2007 6th IEEE and ACM international symposium on mixed and augmented reality*. IEEE, 2007, pp. 225–234.

[19] J. Engel, V. Koltun, and D. Cremers, "Direct sparse odometry," *IEEE transactions on pattern analysis and machine intelligence*, vol. 40, no. 3, pp. 611–625, 2017.

[20] S. Yang and S. Scherer, "Monocular object and plane slam in structured environments," *IEEE Robotics and Automation Letters*, vol. 4, no. 4, pp. 3145–3152, 2019.

[21] L. Nicholson, M. Milford, and N. Sünderhauf, "Quadricslam: Dual quadrics from object detections as landmarks in object-oriented slam," *IEEE Robotics and Automation Letters*, vol. 4, no. 1, pp. 1–8, 2018.

[22] A. Rosinol, M. Abate, Y. Chang, and L. Carlone, "Kimera: an open-source library for real-time metric-semantic localization and mapping," in *2020 IEEE International Conference on Robotics and Automation (ICRA)*. IEEE, 2020, pp. 1689–1696.

[23] H. Huang, L. Li, H. Cheng, and S.-K. Yeung, "Photo-slam: Real-time simultaneous localization and photorealistic mapping for monocular stereo and rgb-d cameras," in *Proceedings of the IEEE/CVF Conference on Computer Vision and Pattern Recognition*, 2024, pp. 21 584–21 593.

[24] N. Keetha, J. Karhade, K. M. Jatavallabhula, G. Yang, S. Scherer, D. Ramanan, and J. Luiten, "Splatam: Splat, track & map 3d gaussians for dense rgb-d slam," in *Proceedings of the IEEE/CVF Conference on Computer Vision and Pattern Recognition*, 2024.

[25] P. Z. X. Li, S. Karaman, and V. Sze, "Gmmap: Memory-efficient continuous occupancy map using gaussian mixture model," *IEEE Transactions on Robotics*, vol. 40, pp. 1339–1355, 2024.

[26] K. Wang, W. Ding, and S. Shen, "Quadtree-accelerated real-time monocular dense mapping," in *2018 IEEE/RSJ International Conference on Intelligent Robots and Systems (IROS)*. IEEE, 2018, pp. 1–9.

[27] J. L. Schönberger and J.-M. Frahm, "Structure-from-motion revisited," in *Conference on Computer Vision and Pattern Recognition (CVPR)*, 2016.

[28] J. L. Schönberger, E. Zheng, M. Pollefeys, and J.-M. Frahm, "Pixel-wise view selection for unstructured multi-view stereo," in *European Conference on Computer Vision (ECCV)*, 2016.

[29] P. F. Felzenszwalb and D. P. Huttenlocher, "Efficient belief propagation for early vision," *International journal of computer vision*, vol. 70, pp. 41–54, 2006.

[30] D. Min, S. Choi, J. Lu, B. Ham, K. Sohn, and M. N. Do, "Fast global image smoothing based on weighted least squares," *IEEE Transactions on Image Processing*, vol. 23, no. 12, pp. 5638–5653, 2014.

[31] B. Eckart, K. Kim, A. Troccoli, A. Kelly, and J. Kautz, "Accelerated generative models for 3d point cloud data," in *Proceedings of the IEEE conference on computer vision and pattern recognition*, 2016, pp. 5497–5505.

[32] C. O'Meadhra, W. Tabib, and N. Michael, "Variable resolution occupancy mapping using gaussian mixture models," *IEEE Robotics and Automation Letters*, vol. 4, no. 2, pp. 2015–2022, 2018.

[33] A. Dhawale and N. Michael, "Efficient parametric multi-fidelity surface mapping," in *Robotics: Science and Systems (RSS)*, vol. 2, no. 3, 2020, p. 5.

[34] K. Goel, N. Michael, and W. Tabib, "Probabilistic point cloud modeling via self-organizing gaussian mixture models," *IEEE Robotics and Automation Letters*, vol. 8, no. 5, pp. 2526–2533, 2023.

[35] S. R. Bulò, L. Porzi, and P. Kontschieder, "Revising densification in gaussian splatting," *arXiv preprint arXiv:2404.06109*, 2024.

[36] J. Straub, T. Whelan, L. Ma, Y. Chen, E. Wijmans, S. Green, J. J. Engel, R. Mur-Artal, C. Ren, S. Verma, *et al.*, "The replica dataset: A digital replica of indoor spaces," *arXiv preprint arXiv:1906.05797*, 2019.

[37] J. Sturm, N. Engelhard, F. Endres, W. Burgard, and D. Cremers, "A benchmark for the evaluation of rgb-d slam systems," in *Proc. of the International Conference on Intelligent Robot Systems (IROS)*, Oct. 2012.

[38] Z. Teed and J. Deng, "Raft: Recurrent all-pairs field transforms for optical flow," in *Computer Vision–ECCV 2020: 16th European Conference, Glasgow, UK, August 23–28, 2020, Proceedings, Part II 16*. Springer, 2020, pp. 402–419.